Nanoscale

PAPER

View Article Online
View Journal

Cite this: DOI: 10.1039/c9nr02173f

Photonic crystallization of two-dimensional MoS_2 for stretchable photodetectors†

Richard Hahnkee Kim,[a,b] Juyoung Leem,[c] Christopher Muratore,[d] SungWoo Nam,[c] Rahul Rao,[a,e] Ali Jawaid,[a,e] Michael Durstock,[a] Michael McConney,[a] Lawrence Drummy,[a] Rachel Rai,[a,d] Andrey Voevodin[f] and Nicholas Glavin *[a]

Received 12th March 2019,
Accepted 7th June 2019

DOI: 10.1039/c9nr02173f

rsc.li/nanoscale

Low temperature synthesis of high quality two-dimensional (2D) materials directly on flexible substrates remains a fundamental limitation towards scalable realization of robust flexible electronics possessing the unique physical properties of atomically thin structures. Herein, we describe room temperature sputtering of uniform, stoichiometric amorphous MoS_2 and subsequent large area (>6.25 cm^2) photonic crystallization of 5 nm 2H-MoS_2 films in air to enable direct, scalable fabrication of ultrathin 2D photodetectors on stretchable polydimethylsiloxane (PDMS) substrates. The lateral photodetector devices demonstrate an average responsivity of 2.52 μW A^{-1} and a minimum response time of 120 ms under 515.6 nm illumination. Additionally, the surface wrinkled, or buckled, PDMS substrate with conformal MoS_2 retained the photoconductive behavior at tensile strains as high as 5.72% and over 1000 stretching cycles. The results indicate that the photonic crystallization method provides a significant advancement in incorporating high quality semiconducting 2D materials applied directly on polymer substrates for wearable and flexible electronic systems.

Introduction

Flexible and stretchable photodetector devices based on two-dimensional (2D) materials are known to exhibit a rare combination of high optoelectronic performance with the ability to accommodate large amounts of strain.[1–6] This unique coupling is enabled by the broad optical absorption in graphene and other 2D material systems, quantum confinement of energy carriers in the 2D plane resulting in ultrafast transport dynamics, the van der Waals bonding between the layers, and the enhanced electromechanical properties that arise due to the extreme thinness of the material.[7,8] Resultant 2D material photodetector devices exhibit rapid photoresponse,[5,6,9,10] semitransparency,[11,12] and even strainability as high as 200% in crumpled systems.[13,14] Practical realization of flexible 2D materials in these applications is primarily limited by the lack of large area, transfer-free processing schemes that enable incorporation of the layered materials onto soft, organic substrates and allow for bottom-up device fabrication. Large scale photonic crystallization of amorphous precursors to layered 2D materials directly on soft substrates, as demonstrated in this study, can facilitate the future 2D flexible electronic and optoelectronics that are easily processed at low temperatures for devices including ultra-thin photodetectors.

Synthesis of 2D materials with high crystal quality typically require high temperatures in the range of 500–1000 °C coupled with an epitaxial template[15] to facilitate the thermodynamic reactions of stoichiometric materials with low defect densities.[16] To overcome the processing limitations for flexible electronics where the substrate typically cannot accommodate for either of these conditions, the 2D layers must either be grown as polycrystalline films at a much lower substrate temperature,[17,18] transferred from a rigid substrate to the flexible substrate of interest,[19–21] or processed by non-thermal annealing techniques in order to achieve similar device performance. Recently, techniques including additive manufacturing have emerged that allow for the transfer of liquid-based

[a]Air Force Research Laboratory, Materials and Manufacturing Directorate, Wright-Patterson AFB, OH 45433, USA. E-mail: Nicholas.Glavin.1@us.af.mil
[b]National Research Council, Washington, D.C. 20418, USA
[c]Department of Mechanical Science and Engineering, University of Illinois at Urbana-Champaign, Urbana, IL 61801, USA
[d]University of Dayton, Dayton, OH 45409, USA
[e]UES, Inc., Dayton, OH 45432, USA
[f]Department of Materials Science and Engineering, University of North Texas, Denton, TX 76203, USA

†Electronic supplementary information (ESI) available: The accompanied supporting information includes thickness measurement of deposited MoS_2 films *via* TEM, XPS characterization before and after annealing, SEM images of film morphology, photodetector performance, Raman analysis under strain, and a comparison to other published results on MoS_2 photodetectors. See DOI: 10.1039/c9nr02173f

2D inks onto flexible substrates for device manufacturing.[5,6,22] These 3D printing approaches enable patternability and low temperature solution processing, however issues with repeatability and film discontinuity require advances before practical devices can be achieved.

Herein, we present a technique that utilizes a large area pulsed light source in order to initiate controllable transformation of amorphous ultrathin MoS_2 films to layered 2H-MoS_2 on flexible polydimethylsiloxane (PDMS). The phase transformation in this case is performed in open air environment and occurs through absorption of the incident light resulting in selective, local heating of the film to temperatures predicted as high as 390 °C without decomposition of the PDMS substrate. Photonic crystallization has been utilized to process materials including graphene inks,[23,24] metallic nanoparticles,[25] and other nanomaterials.[26] This work highlights photonic crystallization as a process to induce phase transformations in semiconductor 2D materials directly on soft stretchable substrates for flexible photo-devices which can operate under repeated stretching cycles.

Results and discussion

The growth and photonic crystallization process that enabled the 2D MoS_2 to be directly synthesized on a flexible polymer substrate are depicted schematically in Fig. 1a. Initially, the flexible and stretchable PDMS substrates (2.5 cm × 2.5 cm and 0.25 cm thickness) were loaded into an ultra-high vacuum plasma reactor with a residual base pressure of 10^{-9} Torr. Room temperature magnetron sputtering from a polycrystalline MoS_2 target yielded continuous large area coverage of the entire PDMS wafer with stoichiometric, amorphous MoS_2 films (X-Ray Photoelectron Spectroscopy data in ESI Fig. S2†). These films served as precursors for subsequent large area crystallization which was performed with a broadband pulsed flash lamp (Pulse Forge 1300 system) to a resulting crystalline film thickness of 5 nm. This process uses high power (1000–2000 W cm^{-2}), short duration (100–300 μs) pulses of broadband light (200–1500 nm) to illuminate a large area on the order of 1 m^2 for thermally processing of thin films. With this specifically tuned photonic curing process, the amorphous MoS_2 films can be thermally crystallized to the 2H semiconducting phase of MoS_2 on the surface of a PDMS substrate without evidence of substrate decomposition. Previous studies of laser annealing indicate that the transformation is mostly thermal, as the crystallization is dependent upon irradiance (*i.e.* power and time) rather than strictly fluence.[27] Crystallization over the entire surface of the 6.25 cm^2 samples was uniform as evidence by spatially-resolved micro-Raman spectroscopy, with only slight changes in morphology at the extreme edges (less than 50 μm) likely due to enhanced cooling at the sample edges (ESI Fig. S3†).

The Raman spectra (514.5 nm excitation) of PDMS, amorphous MoS_2, and crystalline MoS_2 in Fig. 1b reveal the presence of the peak associated with in-plane stretching of 2H MoS_2 mode at 383 cm^{-1} (E^1_{2g}) and the peak for out-of-plane stretching around 406 cm^{-1} (A_{1g}), which are only visible after the photonic crystallization. Polarized Raman spectra in the cross-polarized configuration (see Experimental methods for more detailed explanation) provide clues to the orientation of the MoS_2 layers. In a backscattering configuration, the out-of-plane A_{1g} mode is expected to disappear for the cross-polarized configuration, which can observed for transition metal dichalcogenide (TMD) layers parallel to the substrate[28] but not when they are aligned at other angles.[29] The polarized Raman spectra from the photonically crystallized films shows a significant decrease in intensity of the A_{1g} mode relative to the E^1_{2g} mode, therefore strongly suggesting the presence of MoS_2 layers crystallized parallel to the substrate.

As shown in Fig. 1c both the amorphous and crystalline MoS_2 on the PDMS substrate exhibit similar semitransparency to visible light. Absorbance spectra reveal that the initial amorphous film is featureless with no observable exciton peaks characteristic of crystalline 2D MoS_2. The spectra of photonically crystallized MoS_2 resolves electronic transitions at 602 nm and 398 nm, consistent with B and C excitonic transitions.[30] The broadness of the direct excitonic features may be due to defect states present in the polycrystalline MoS_2. As these excitonic transitions are highly localized,[31,32] the strength of these electronic transitions can be attenuated due to defect trap-state recombination sites.

The magnetron sputtering and photonic crystallization process results in a uniform nanocrystalline MoS_2 coating over the polymer substrate. Cross-sectional TEM imaging reveals a continuous layered structure with a film thickness of 5 nm (Fig. S1†). The morphology of the film and substrate is dominated by buckles on the surface of the PDMS upon exposure to both the film deposition processes and the photonic crystallization.[33] Two-dimensional graphene and TMD materials have been known to "crumple" or "wrinkle" under an applied compressive load, which has been shown to improve both the mechanical properties and photodetector properties.[13,14] The evolution of the buckled topography of the MoS_2/PDMS system is shown in Fig. 2a. Initially prior to any MoS_2 processing or deposition, the PDMS is nearly atomically smooth with an RMS roughness of 0.04 nm. The coupled processes of exposure to vacuum and energetic plasma species during amorphous MoS_2 deposition increases the RMS roughness to 4.32 nm and periodic surface wrinkles of around 200 nm in diameter are prevalent over the entire surface. This surface wrinkling and buckling has been known to occur during ultra-high vacuum deposition by a combination of exposure to vacuum condition as well as plasma bombardment during the growth process, allowing for bulging at the MoS_2/PDMS interface.[33,34] Upon crystallization, the local heating within the MoS_2 and the coefficient of thermal expansion mismatch between the two interfaces results in surface wrinkling with larger diameters approaches 1 μm as well as an increase in the RMS roughness to 9.16 nm. It is notable that previous studies observed a change in the morphology of MoS_2 after laser annealing to aligned crystallites, where the photonic curing in

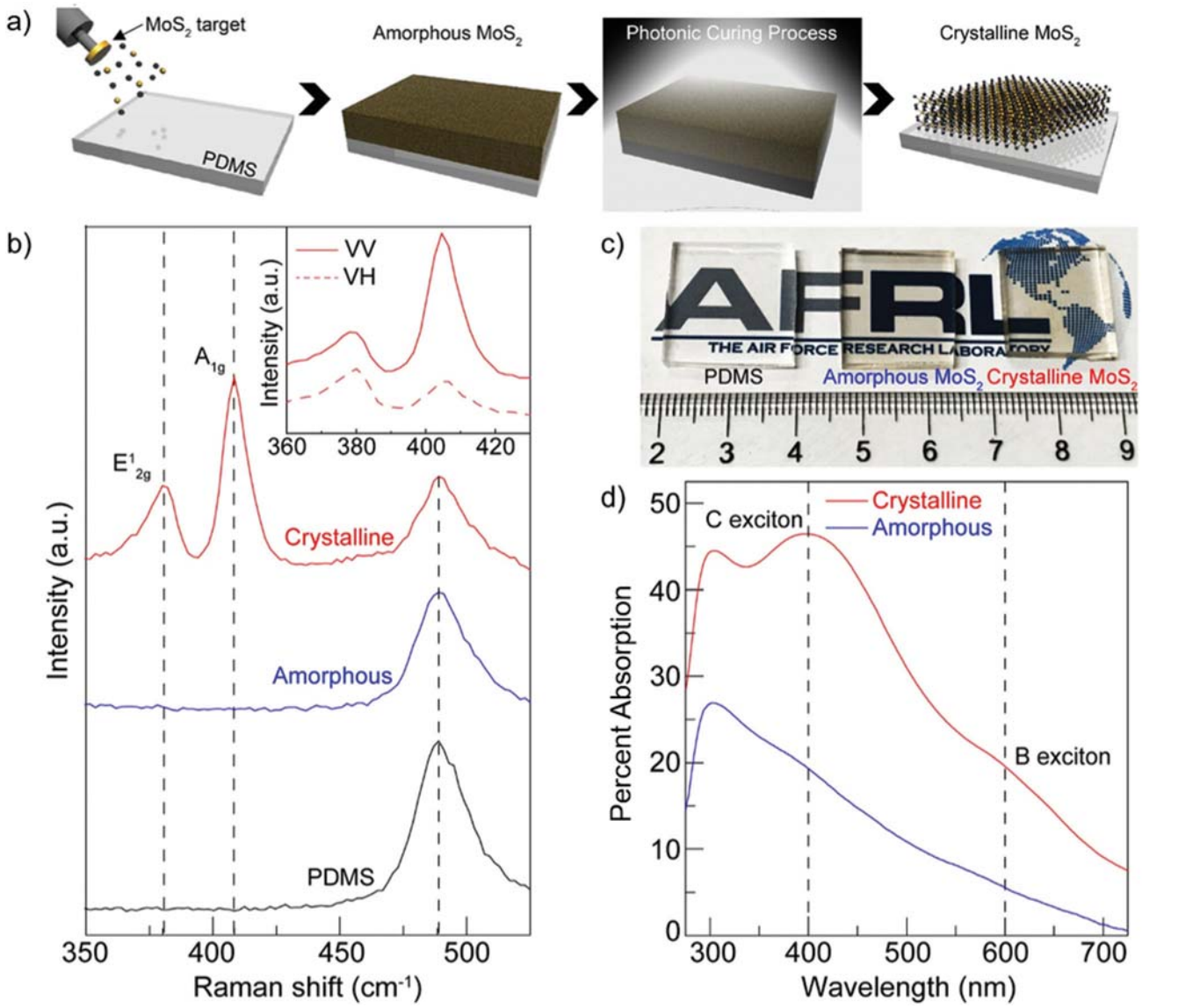

Fig. 1 Photonic crystallization and characterization of MoS_2 films. (a) Schematic diagram depicting the fabrication of the crystalline MoS_2 films on the PDMS substrate with the photonic curing process, (b) Raman scans of PDMS substrate, amorphous MoS_2 and crystalline MoS_2 with the inset spectra depicting polarized scans in the parallel (VV) and cross-polarized (VH) direction, (c) optical image of samples; bare PDMS, amorphous MoS_2 films on the PDMS, and crystalline MoS_2 films on the PDMS (from left), and (d) comparison of the absorption behavior between amorphous MoS_2 films and crystalline MoS_2 films on the PDMS substrate. Logo courtesy of AFRL.

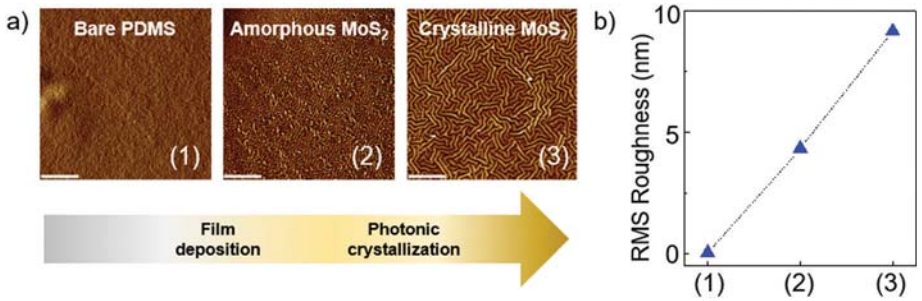

Fig. 2 MoS_2/PDMS surface morphology. (a) AFM surface scans of bare PDMS, amorphous MoS_2 on PDMS, and crystalline MoS_2 on PDMS with scale bars of 5 μm, and (b) RMS roughness of the films at the same conditions.

this case resulted in random and isotropic morphology.[27] The use of photonic crystallization rather than laser-based approaches allows for large area industrially scalable processing with relatively low equipment cost relative to a larger laser setup. Additionally, the uniform thermal heating across the wafer provides for uniform buckling across the wafer except at the extreme edges (shown in ESI Fig. S3†). The buckled nature of PDMS and uniform coating of MoS_2 from the deposition process are presumed to be key enablers to stretchability in the photodetector demonstrations described later.[35] This controlled buckling phenomena in PDMS results from several mechanisms including vacuum exposure, plasma interaction, and thermal mismatch, and can potentially be controlled and tailored for future stretchability enhancement.[36,37]

The threshold for photonic crystallization in the amorphous films was identified by systematic investigation of the applied photonic energy fluence and broadband light pulse duration. Raman intensity of the A_{1g} peak post-annealing at different pulse energies and times is shown in Fig. 3a. For the case of 5 nm MoS_2 on PDMS, the optimal range for crystallization is within a photonic pulse duration of 125 μs to 300 μs and fluence of 0.85 to 1.20 J cm^{-2} and with a step size between sample conditions of ~0.1 J cm^{-2} and 50 microseconds. The condition in which the A_{1g} peak was most intense for the photonically crystallized MoS_2 films occurred under an illumination energy of 1.14 J cm^{-2} and 250 μs pulse time. At these conditions, the linewidth of the A_{1g} peak was 10.1 cm^{-1}, indicating that the grain size is in the tens of nanometers.[38] Above a particular threshold of incident energy, and the heat generated from incident light source in the MoS_2 layer coupled with the large coefficient of thermal expansion mismatch caused film cracking and delamination of the MoS_2 film from the PDMS substrate (ESI Fig. S5†). After this point, the films were not electrically continuous and could not be evaluated in large area optical device tests. Raman studies indicate that the film within these cracked areas are in fact crystalline and controlling the crack formation/delamination process is critical for high quality films. The MoS_2 thickness of 5 nm was utilized in this study due to the strong absorption at that material thickness, and future experiments on thinner films (especially approaching monolayer) will require larger lamp sources with higher power outputs to achieve similar local temperatures.

The peak temperature in both the amorphous MoS_2 film and the top layer of PDMS during the rapid annealing process were estimated using SimPulse software thermal modeling (NovaCentrix) for a 5 nm MoS_2 on 1 mm PDMS substrate. The modeling software considers first principles approaches coupled with the magnitude and time characteristics of the photonic pulse of light, the material absorption properties at the broadband wavelengths (from Fig. 1d), and relevant material properties including thermal conductivity and specific heat. Fig. 3b depicts the estimated transient temperature of the MoS_2 during crystallization for selected illumination energy fluences. The process conditions described above for the highest degree of crystallization resulted in a peak estimated temperature of 390 °C (denoted by the star in Fig. 3b).

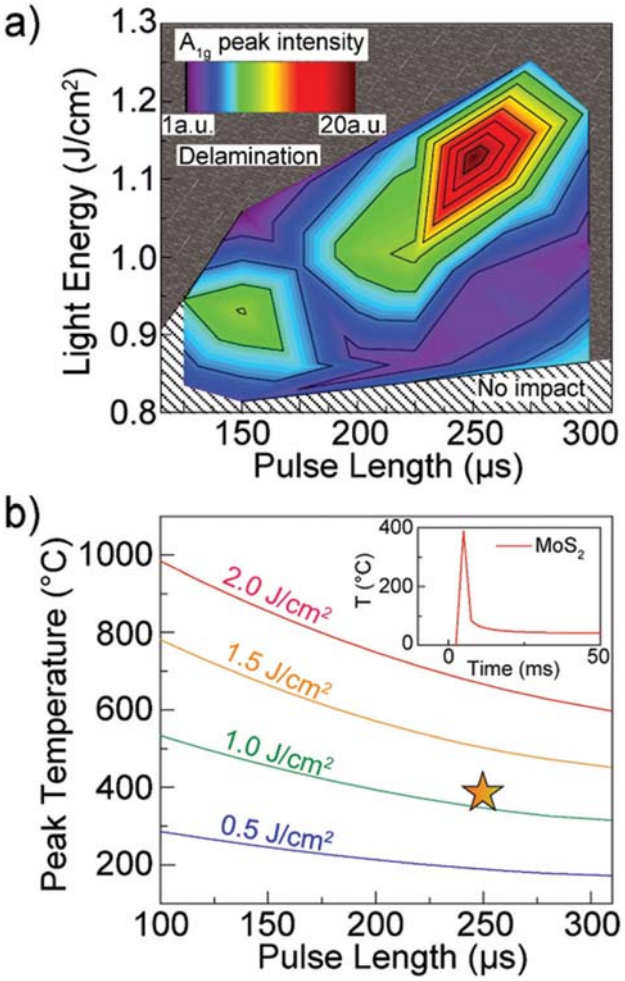

Fig. 3 Optimization of the photonic crystallization process. (a) Raman intensity of the A_{1g} peak post-annealing at different pulse energies and times, (b) the estimated transient temperature of the MoS_2 during crystallization for selected illumination energy densities and inset depicts the temporal thermal profile of the MoS_2 at the optimal annealing conditions (1.14 J cm^{-2} and 250 μs pulse length).

This is a critical observation in that the onset of decomposition of PDMS occurs around 250 °C,[39] which highlights the benefits of selective and transient heating from the photonic curing technique as we do not observe decomposition within the polymer at the appropriate conditions. A modeled temporal thermal profile of the MoS_2 is shown in the inset in Fig. 3b depicts the film cooling from as peak temperature of 390 °C to room temperature within 25 ms. In previous works, growth and crystallization of MoS_2 occurred at temperatures above 350 °C on SiO_2 substrates, in the same range as the temperature predicted by the Simpulse model software.[38,40] Additionally, the MoS_2 films reveal partial oxidation observed in the XPS analysis after illumination (ESI Fig. S2†), indicating that the temperature of the film during photonically induced crystallization exceeded 330 °C, which was the critical temperature reported for MoS_2 decomposition in air.[41,42] From these observations, future photonic crystallization experiments con-

ducted in inert ambient environments (*i.e.*, argon gas) are necessary to entirely reduce or eliminate oxidation. The low thermal conductivity of the amorphous film material and the polymer substrate assist in isolating the heat in the film, as do the significant interfacial elastic modulus mismatch resulting in low interfacial thermal conductance. The film/substrate interface does not reach these high temperatures due to transient heating and poor interfacial thermal transport, indicating that the photonic annealing is considerably more advantageous than conventional heating.

To evaluate the feasibility of the photonically crystallized MoS_2 for flexible devices, lateral photodetector devices were fabricated with Ti/Au contacts forming a 10 μm channel length, as shown in the inset of Fig. 4a. Under illumination of 515.6 nm wavelength laser (spot size 100 μm estimated by the razor blade method) over the entire device channel, laser power dependent photocurrent was observed with an applied external bias voltage of 1 V as shown in Fig. 4b. The increase in photocurrent is a direct result of photo-induced carriers within the active device region, indicating semiconductor device quality material over many micrometers. Our device results in Fig. 4b depict a relatively constant photoresponsivity *versus* laser intensity, implying that photovoltaic mode is dominant in photocurrent generation.[43,44] This is determined by the relationship between photocurrent and incident laser power in the expression $I_{ph} \propto P^{\gamma}$, where a γ value of 1 indicates photodetector performance dominated by the photovoltaic effect rather than photothermal effect (Fig. S8†). The conductivity of the MoS_2 channel in dark mode is estimated at 9.1 Ω^{-1} cm^{-1}, which is a relatively high for a thin film MoS_2 and the conductivity increase of the MoS_2 channel with laser illumination of 59.84 W cm^{-2} was 1.2 Ω^{-1} cm^{-1}.[45] Overall, the photoresponsivity of our device without the inclusion of any dark current contributions averaged 2.52 μA W^{-1} and maintained a constant value while the laser power increased from 4.71 W cm^{-2} to 59.8 W cm^{-2}.

The time-resolving, dynamic on/off behavior of the device is shown in Fig. 4c as the illumination is cycled on and off, with rise and fall times (within 10% of maximum and minimum current) of 240 and 214 ms, respectively, as shown in Fig. 4d, at the highest laser power tested. The fastest response time was observed at the lowest laser power, with a rise and fall time of 122 and 120 ms, respectively (a full set of rise time and fall time analysis is shown in ESI Table S1†). The performance of our photodetector device with photonically crystallized MoS_2 films is lower in absolute responsivity in comparison to previous works of visible photodetectors made of single- or few-layer TMDs (ESI Table 2†), but the response time is comparable and the ease of processing and direct on polymer synthesis makes the approach very enticing for future device fabrication.[46–57] As multi-layer MoS_2 is an indirect bandgap semiconductor, the photocurrent amplitude is reduced in comparison to devices fabricated from single 2D layers and is also sensitive to the presence of defects and impurities. It is anticipated that further developments in the photonic annealing process (employing an inert atmosphere, reducing layer thickness, *etc.*) will improve photoresponse and device performance even further.

To demonstrate the utility of direct fabrication and creation of this buckled topography of our photonically crystalized 2D

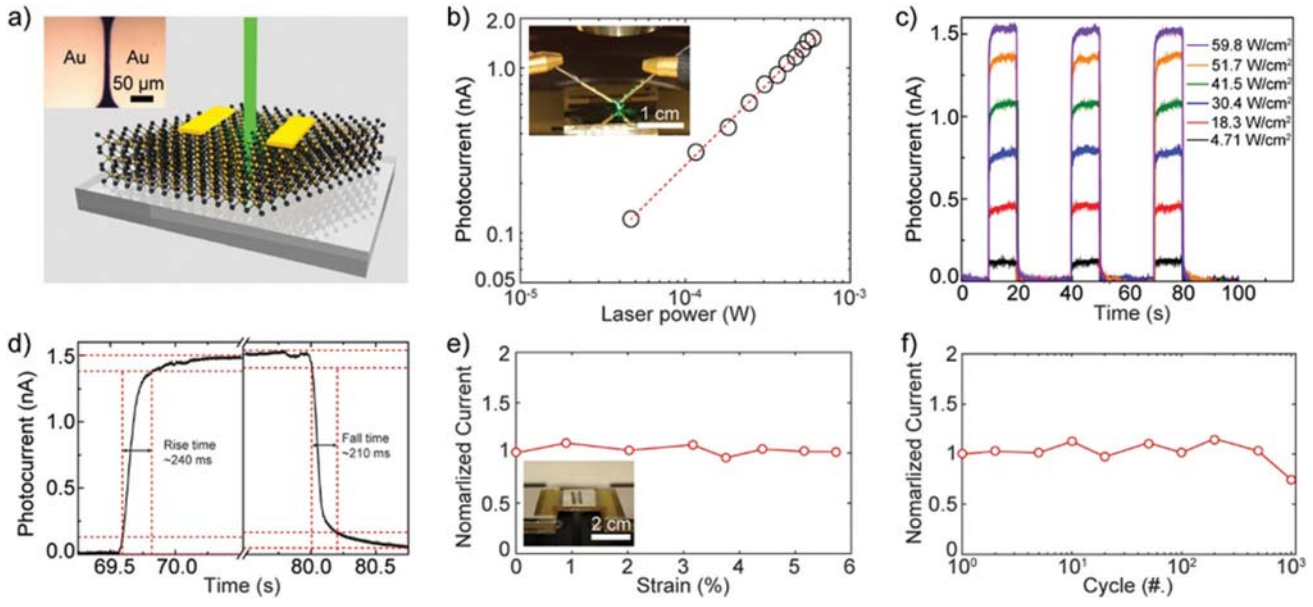

Fig. 4 2D MoS_2 photodetector performance. (a) A schematic representation of 2D MoS_2 photodetector with a laser illumination. Inset: An optical microscopic image of the actual device. (b) Power dependent photocurrent measured from fabricated MoS_2 photodetector. Inset: A photograph of the photocurrent measurement setup with the laser illumination. (c) Time-resolved photocurrent measured from the MoS_2 photodetector. (d) Rise time and fall time of the photocurrent measurement, (e) normalized current measured from the device under the range of tensile strain, from 0 to 5.72% and inset image of the stretching setup, and (f) mechanical durability of the fabricated device from cyclic testing.

photodetectors for stretchable electronics, the devices were measured under the range of tensile strains from 0% to 5.72% as well as 1000 cycles of stretching–releasing tests. The MoS_2 photodetector on PDMS was mounted on a stretching stage which allows precise strain control using a micromanipulator, and the photocurrent was measured under different tensile strains. In Fig. 4e, the measured photocurrent was normalized with the photocurrent value measured with no externally applied tensile strain. The normalized photocurrent remained constant up to 5.72% tensile strain, suggesting the material system remains stable under the range of applied tensile strain. Beyond this strain, the sample continuously detached from the stretching stage and could have sustained further stretching with a more robust mounting setup. Raman spectra collected under the same applied strain also show the expected changes in peak frequencies and linewidths (ESI Fig. S9†) indicating that the MoS_2 is undergoing some strain during the stretching process. We attribute the performance stability in the devices under stretching to the uniform coating over the buckled PDMS surface, coupled with the inherent flexibility of the 2D semiconducting MoS_2.

In addition to examining the maximum tensile load, mechanical durability of the fabricated device was also demonstrated with the MoS_2 photodetector mounted to the stretching stage. The generated photocurrent from the device was measured in the unstrained condition periodically over 1000 cycles of 4% tensile strain applied. The photocurrent values were normalized with the photocurrent value measured after one cycle of stretching–releasing, and the normalized current is displayed in Fig. 4f. The resulting current level is consistent over 1000 cycles of stretching–releasing, with a minor decrease of 25% near the conclusion of the experiment. This result implies that MoS_2 can be further fabricated into stretchable devices with mechanical robustness for repeated cycling during use in applications such as wearable and flexible electronics.

Conclusion

In summary, we demonstrated a large area and low temperature 2D material synthesis platform through room temperature sputtering and photonic crystallization of 5 nm MoS_2 films directly on a polymer substrate for flexible and stretchable optoelectronics. The phase transformation of amorphous to polycrystalline 2H MoS_2 occurs through absorption of the incident broadband light resulting in selective, local heating of the film to temperatures sufficiently high to induce crystallization, but not induce decomposition of the PDMS substrate. The crystalline MoS_2 on the PDMS substrate was readily then employed in a lateral, two-terminal photodetector exhibiting a linear responsivity with respect to the laser power of 2.52 $\mu A\,W^{-1}$ and a minimum response time of 120 ms upon illumination with 515.6 nm laser excitation. Furthermore, the photodetectors were mechanically stretchable up to 5.72% strain and over 1000 cycling events at a tensile strain of 4%. The results described in this study indicate that photonic crystallization may be an effective integration strategy for large area semiconducting 2D materials on stretchable and flexible substrates suitable for a new generation of electronics.

Experimental methods

PDMS substrate preparation and deposition of amorphous MoS_2

An elastomeric PDMS substrate was fabricated by curing a PDMS precursor (Sylgard 184, Dow Corning Corp) on a smooth silicon wafer in a dish. We used a mixture of PDMS precursor and curing agent (10 : 1 by weight) that had been degassed under vacuum. After the PDMS mixture was cured at 60 °C for 6 h using a vacuum oven, the PDMS was peeled off from the Si wafer. Then the substrates were cut up into smaller pieces (2.5×2.5 cm^2). The surface that was cast onto the flat silicon surface to form an extremely flat PDMS substrate for deposition. The PDMS samples were introduced *via* a vacuum load-lock and mounted on an electrically grounded fixture. Substrates were rotated at a rate of approximately 100 rpm while positioned 7 cm from the MoS_2 target. The synthesis chamber was pumped to a base pressure of $<10^{-9}$ Torr and was then filled with ultra-high purity argon gas at a constant flow rate of 25 sccm to a pressure of 10 mTorr. All MoS_2 films were grown at room temperature *via* magnetron sputtering using a solid 3.3 cm diameter MoS_2 target of 99.95% purity. Pulsed dc power (60 W at 65 kHz) was applied to the MoS_2 target to initiate the sputtering process.

Photonic curing of MoS_2

The photonic crystallization was performed on a PulseForge 1300 photonic curing system manufactured by NovaCentrix. Processing parameters such as the fluence, pulse length, and the temporal evolution of the pulse shape were controlled to obtain the optimized annealing condition to crystallize amorphous MoS_2 films on PDMS substrate.

Characterization

The backscattered Raman spectra were acquired with a Renishaw in *Via* Raman Microscope using 514.5 nm excitation. The incident laser power was kept below 1 mW to avoid heating of the samples. Parallel- and cross-polarized Raman spectra (denoted as VV and VH, respectively, where V and H are the vertical and horizontal electric field vectors of the incident excitation laser) were also collected in the backscattering configuration from the crystallized MoS_2. Compositional changes in the MoS_2 films associated with the photonic annealing process were characterized *via* X-ray Photoelectron Spectroscopy (XPS). Scans were collected with a Surface Science Instruments M-Probe XPS system equipped with a monochromatic Al Kα X-ray source (photon energy of 1486.7 eV) operated at 50 W. All peak positions were calibrated to an adventitious carbon C 1s peak value of 284.5 eV. Analysis was

based on the position of the peaks, their area, and their full width half maximum with fitted to a Shirley background.

UV-Vis spectra were acquired on a CRAIC UV-Vis optical microscope with a spot size of 10 micorns. Blank PDMS were taken as reference spectra and spectra were acquired using 16 ms dwell time and averaged over 16 spectra.

Atomic force microscopy profiles

Images were obtained in non-contact mode with an Antimony coated Si probe (force constant = 0.01 N m^{-1}). Scale bars are 5 micron. Surface roughness measurements were performed after performing a tilt correction to account for sample drift. MoS_2 film heights were measured by masking a portion of the PDMS substrate, MoS_2 deposited, and removal of the mask. The height difference between unmasked and deposited film were taken as film thicknesses. All images were processed using Bruker Nanoscope Analysis Software.

SimPulse modeling of transient temperature profiles

Simpulse modeling software was provided by the PulseForge 1300 photonic curing system manufacturing by NovaCentrix. Input to the simulation was the creation of a simulated layer structure with 5 nm MoS_2 and 1 mm thick PDMS substrate. The average absorption properties from MoS_2 (12% absorption) gathered from Fig. 1d and thermal properties of amorphous MoS_2 were used from previous works.[38] The broadband light source spectrum can be found on the company website and further details with regards to the Simpulse software.

Photodetector fabrication and photocurrent measurement

Metal electrodes (Ti/Au: 25 nm/50 nm) were deposited on the fabricated MoS_2 on PDMS by e-beam evaporator (Temescal FC-2000 electron beam evaporator Ferrotec USA, CA) at 2.5 × 10^{-6} Torr with a shadow mask. The dimension of photodetector is defined by the shadow mask's window size.

To characterize the photoresponse of the fabricated MoS_2 photodetector array photocurrent was measured with a diode laser (515.6 nm, Thorlab, NJ), a sourcemeter (Keithley 2614B, Tektronix, OR), and microprobe station. Laser power dependent photocurrent was measured under the range of laser power, from 4.8 mW to 0.4 mW. The diameter of laser spot was approximately 100 μm measured by the razor blade method.

Photodetector fabrication for strain independent photoresponse measurement

Metal electrodes (Ti/Au: 25 nm/50 nm) were deposited on the fabricated MoS_2 on PDMS by e-beam evaporator (Temescal FC-2000 electron beam evaporator Ferrotec USA, CA) at 2.5 × 10^{-6} Torr with a shadow mask, under a bending strain (~10% tensile strain). To avoid possible breakage at metal electrodes while the tensile strain was applied, the metal electrode was deposited under a tensile strain higher than the maximum strain employed for photocurrent measurements. After deposition, the bending strain was released, and the photodetector array sample was mounted on a stretching stage. Using the stretching stage, tensile strain was applied to the sample, and photocurrent was measured in the range of tensile strains, from 0% to 5.72%. For durability test, the sample was repeatedly stretched and released for 1000 cycles, with the maximum tensile strain of 4%. Photocurrent was measured at 1, 2, 5, 10, 20, 50, 100, 200, 500, 1000th cycle to show the consistency.

Conflicts of interest

There are no conflicts to declare.

Acknowledgements

The authors would like to thank Art Safriet of University of Dayton Research laboratory initial design of the deposition chamber. Additionally, the authors would like to acknowledge TEM preparation and imaging support from Scott Apt and Melinda Ostendorf. S. N. gratefully acknowledges support from the AFOSR (FA9550-16-1-0251 and FA2386-17-1-4071), NSF-MRSEC (DMR-1720633) and NASA ECF (NNX16AR56G). E-beam deposition and a part of the device fabrication process was carried out in the Materials Research Laboratory Central Research Facilities at the University of Illinois at Urbana-Champaign. This research was performed while the author held an NRC Research Associateship award at Wright-Patterson Air Force Research Laboratory.

References

1 S. J. Kim, K. Choi, B. Lee, Y. Kim and B. H. Hong, Materials for Flexible, Stretchable Electronics: Graphene and 2D Materials, *Annu. Rev. Mater. Res.*, 2015, **45**, 63–84.
2 D. De Fazio, I. Goykhman, D. Yoon, M. Bruna, A. Eiden, S. Milana, U. Sassi, M. Barbone, D. Dumcenco, K. Marinov, A. Kis and A. C. Ferrari, High Responsivity, Large-Area Graphene/MoS2 Flexible Photodetectors, *ACS Nano*, 2016, **10**, 8252–8262.
3 P. T. Gomathi, P. Sahatiya and S. Badhulika, Large-Area, Flexible Broadband Photodetector Based on ZnS–MoS2 Hybrid on Paper Substrate, *Adv. Funct. Mater.*, 2017, **27**, 1701611–n/a.
4 C. Xie, C. Mak, X. Tao and F. Yan, Photodetectors Based on Two-Dimensional Layered Materials Beyond Graphene, *Adv. Funct. Mater.*, 2017, **27**, 1603886–n/a.
5 L. Jinseong, K. Richard Hahnkee, Y. Seunggun, V. Dhinesh Babu, L. Hyeokjung, P. Chanho, C. Suk Man, J. Beomjin, K. Han Sol and P. Cheolmin, Design of amine modified polymer dispersants for liquid-phase exfoliation of transition metal dichalcogenide nanosheets and their photodetective nanocomposites, *2D Mater.*, 2017, **4**, 041002.
6 D. B. Velusamy, R. H. Kim, S. Cha, J. Huh, R. Khazaeinezhad, S. H. Kassani, G. Song, S. M. Cho, S. H. Cho, I. Hwang, J. Lee, K. Oh, H. Choi and C. Park, Flexible transition metal dichalcogenide nanosheets for

band-selective photodetection, *Nat. Commun.*, 2015, **6**, 8063.
7 K. F. Mak, C. Lee, J. Hone, J. Shan and T. F. Heinz, Atomically Thin MoS2: A New Direct-Gap Semiconductor, *Phys. Rev. Lett.*, 2010, **105**, 136805.
8 G. Y. Jia, Y. Liu, J. Y. Gong, D. Y. Lei, D. L. Wang and Z. X. Huang, Excitonic quantum confinement modified optical conductivity of monolayer and few-layered MoS2, *J. Mater. Chem. C*, 2016, **4**, 8822–8828.
9 A. Urich, K. Unterrainer and T. Mueller, Intrinsic Reponse Time of Graphene Photodetectors, *Nano Lett.*, 2011, **11**, 2804–2808.
10 F. Bonaccorso, Z. Sun, T. Hasan and A. C. Ferrari, Graphene photonics and optoelectronics, *Nat. Photonics*, 2010, **4**, 611–622.
11 Y.-L. Liu, C.-C. Yu, K.-T. Lin, T.-C. Yang, E.-Y. Wang, H.-L. Chen, L.-C. Chen and K.-H. Chen, Transparent, Broadband, Flexible, and Bifacial-operable Photodetectors Containing a Large-Area Graphene-Gold Oxide Heterojunction, *ACS Nano*, 2015, **9**, 5093–5103.
12 Z. Sun, T. Liao, Y. Dou, S. M. Hwang, M.-S. Park, L. Jiang, J. H. Kim and S. X. Dou, Generalized self-assembly of scalable two-dimensional transition metal oxide nanosheets, *Nat. Commun.*, 2014, **5**, 3813.
13 P. Kang, M. C. Wang, P. M. Knapp and S. Nam, Crumpled Graphene Photodetector with Enhanced, Strain-Tunable, and Wavelength-Selective Photoresponsivity, *Adv. Mater.*, 2016, **28**, 4639–4645.
14 M. Kim, P. Kang, J. Leem and S. Nam, A stretchable crumpled graphene photodetector with plasmonically enhanced photoresponsivity, *Nanoscale*, 2017, **9**, 4058–4065.
15 X. Li, L. Basile, B. Huang, C. Ma, J. Lee, I. Vlassiouk, A. A. Puretzky, M.-W. Lin, M. Yoon, C. Miaofang, J. C. Idrobo, C. M. Rouleau, B. G. Sumpter, D. B. Geohegan and K. Xiao, van der Waals Epitaxial Growth of Two-Dimensional Single-Crystalline GaSe Domains on Graphene, *ACS Nano*, 2015, **9**, 8078–8088.
16 J. Yu, J. Li, W. Zhang and H. Chang, Synthesis of high quality two-dimensional materials via chemical vapor deposition, *Chem. Sci.*, 2015, **6**, 6705–6716.
17 J. Mun, Y. Kim, I.-S. Kang, S. K. Lim, S. J. Lee, J. W. Kim, H. M. Park, T. Kim and S.-W. Kang, Low-temperature growth of layered molybdenum disulphide with controlled clusters, *Sci. Rep.*, 2016, **6**, 21854.
18 A. Delabie, M. Caymax, B. Groven, M. Heyne, K. Haesevoets, J. Meersschaut, T. Nuytten, H. Bender, T. Conard, P. Verdonck, S. Van Elshocht, S. De Gendt, M. Heyns, K. Barla, I. Radu and A. Thean, Low temperature deposition of 2D WS2 layers from WF6 and H2S precursors: impact of reducing agents, *Chem. Commun.*, 2015, **51**, 15692–15695.
19 S. H. Lee, S. Kim, S. Lee and J. S. Yu, Large-area growth of multi-layered MoS2 for violet (~405 nm) photodetector applications, *Phys. Status Solidi A*, 2017, 1700221–n/a.
20 J. Bongkyun, K. Chang-Hyun, C. Seung Tae, K. Kyung-Shik, K. Kwang-Seop, L. Hak-Joo, C. Seungmin, A. Jong-Hyun and K. Jae-Hyun, Damage mitigation in roll-to-roll transfer of CVD-graphene to flexible substrates, *2D Mater.*, 2017, **4**, 024002.
21 Y. Chen, X.-L. Gong and J.-G. Gai, Progress and Challenges in Transfer of Large-Area Graphene Films, *Adv. Sci.*, 2016, **3**, 1500343–n/a.
22 F. Bonaccorso, A. Bartolotta, J. N. Coleman and C. Backes, 2D-Crystal-Based Functional Inks, *Adv. Mater.*, 2016, **28**, 6136–6166.
23 E. B. Secor, T. Z. Gao, M. H. Dos Santos, S. G. Wallace, K. W. Putz and M. C. Hersam, Combustion-assisted Photonic Annealing of Printable Graphene Inks via Exothermic Binders, *ACS Appl. Mater. Interfaces*, 2017, 29418–29423.
24 E. B. Secor, B. Y. Ahn, T. Z. Gao, J. A. Lewis and M. C. Hersam, Rapid and Versatile Photonic Annealing of Graphene Inks for Flexible Printed Electronics, *Adv. Mater.*, 2015, **27**, 6683–6688.
25 H.-J. Hwang, K.-H. Oh and H.-S. Kim, All-photonic drying and sintering process via flash white light combined with deep-UV and near-infrared irradiation for highly conductive copper nano-ink, *Sci. Rep.*, 2016, **6**, 19696.
26 J. Troughton, M. J. Carnie, M. L. Davies, C. Charbonneau, E. H. Jewell, D. A. Worsley and T. M. Watson, Photonic flash-annealing of lead halide perovskite solar cells in 1 ms, *J. Mater. Chem. A*, 2016, **4**, 3471–3476.
27 M. E. McConney, N. R. Glavin, A. T. Juhl, M. H. Check, M. F. Durstock, A. A. Voevodin, T. E. Shelton, J. E. Bultman, J. Hu, M. L. Jespersen, M. K. Gupta, R. D. Naguy, J. G. Colborn, A. Haque, P. T. Hagerty, R. E. Stevenson and C. Muratore, Direct synthesis of ultra-thin large area transition metal dichalcogenides and their heterostructures on stretchable polymer surfaces, *J. Mater. Res.*, 2016, **31**, 967–974.
28 X. Zhang, W. P. Han, J. B. Wu, S. Milana, Y. Lu, Q. Q. Li, A. C. Ferrari and P. H. Tan, Raman spectroscopy of shear and layer breathing modes in multilayer MoS2, *Phys. Rev. B: Condens. Matter Mater. Phys.*, 2013, **87**, 115413.
29 X. Fu, J. Qian, X. Qiao, P. Tan and Z. Peng, Nonlinear saturable absorption of vertically stood WS2 nanoplates, *Opt. Lett.*, 2014, **39**, 6450–6453.
30 L. Wang, Z. Wang, H.-Y. Wang, G. Grinblat, Y.-L. Huang, D. Wang, X.-H. Ye, X.-B. Li, Q. Bao, A.-S. Wee, S. A. Maier, Q.-D. Chen, M.-L. Zhong, C.-W. Qiu and H.-B. Sun, Slow cooling and efficient extraction of C-exciton hot carriers in MoS2 monolayer, *Nat. Commun.*, 2017, **8**, 13906.
31 A. Gurarslan, Y. Yu, L. Su, Y. Yu, F. Suarez, S. Yao, Y. Zhu, M. Ozturk, Y. Zhang and L. Cao, Surface-Energy-Assisted Perfect Transfer of Centimeter-Scale Monolayer and Few-Layer MoS2 Films onto Arbitrary Substrates, *ACS Nano*, 2014, **8**, 11522–11528.
32 Y. Yu, Y. Yu, Y. Cai, W. Li, A. Gurarslan, H. Peelaers, D. E. Aspnes, C. G. Van de Walle, N. V. Nguyen, Y.-W. Zhang and L. Cao, Exciton-dominated Dielectric Function of Atomically Thin MoS2 Films, *Sci. Rep.*, 2015, **5**, 16996.

33 H.-G. Park, H.-C. Jeong, Y. H. Jung and D.-S. Seo, Control of the wrinkle structure on surface-reformed poly(dimethylsiloxane) via ion-beam bombardment, *Sci. Rep.*, 2015, **5**, 12356.

34 D.-S. Um, S. Lim, Y. Lee, H. Lee, H.-J. Kim, W.-C. Yen, Y.-L. Chueh and H. Ko, Vacuum-Induced Wrinkle Arrays of InGaAs Semiconductor Nanomembranes on Polydimethylsiloxane Microwell Arrays, *ACS Nano*, 2014, **8**, 3080–3087.

35 Y. Wang, R. Yang, Z. Shi, L. Zhang, D. Shi, E. Wang and G. Zhang, Super-Elastic Graphene Ripples for Flexible Strain Sensors, *ACS Nano*, 2011, **5**, 3645–3650.

36 S. S. Pandurangi and S. S. Kulkarni, Mechanics of wrinkling of a thin film bonded to a compliant substrate under the influence of spatial thermal modulation, *Int. J. Solids Struct.*, 2015, **62**, 124–133.

37 J.-Y. Park, H. Y. Chae, C.-H. Chung, S. J. Sim, J. Park, H. H. Lee and P. J. Yoo, Controlled wavelength reduction in surface wrinkling of poly(dimethylsiloxane), *Soft Matter*, 2010, **6**, 677–684.

38 C. Muratore, V. Varshney, J. J. Gengler, J. Hu, J. E. Bultman, A. K. Roy, B. L. Farmer and A. A. Voevodin, Thermal anisotropy in nano-crystalline MoS2 thin films, *Phys. Chem. Chem. Phys.*, 2014, **16**, 1008–1014.

39 T. S. Radhakrishnan, Thermal degradation of poly(dimethylsilylene) and poly(tetramethyldisilylene-co-styrene), *J. Appl. Polym. Sci.*, 2006, **99**, 2679–2686.

40 R. A. Vilá, R. Rao, C. Muratore, E. Bianco, J. A. Robinson, B. Maruyama and N. R. Glavin, In situ crystallization kinetics of two-dimensional MoS2, *2D Mater.*, 2017, **5**, 011009.

41 C. Muratore, J. J. Hu, B. Wang, M. A. Haque, J. E. Bultman, M. L. Jespersen, P. J. Shamberger, M. E. McConney, R. D. Naguy and A. A. Voevodin, Continuous ultra-thin MoS2 films grown by low-temperature physical vapor deposition, *Appl. Phys. Lett.*, 2014, **104**, 261604.

42 R. Rao, A. E. Islam, P. M. Campbell, E. M. Vogel and B. Maruyama, In situ thermal oxidation kinetics in few layer MoS2, *2D Mater.*, 2017, **4**, 025058.

43 Y. Zhang, H. Li, L. Wang, H. Wang, X. Xie, S.-L. Zhang, R. Liu and Z.-J. Qiu, Photothermoelectric and photovoltaic effects both present in MoS2, *Sci. Rep.*, 2015, **5**, 7938.

44 V. Patil, A. Capone, S. Strauf and E.-H. Yang, Improved photoresponse with enhanced photoelectric contribution in fully suspended graphene photodetectors, *Sci. Rep.*, 2013, **3**, 2791.

45 L. Yang, P. Liu, J. Li and B. Xiang, Two-Dimensional Material Molybdenum Disulfides as Electrocatalysts for Hydrogen Evolution, *Catalysis*, 2017, **7**, 285.

46 Z. Yin, H. Li, H. Li, L. Jiang, Y. Shi, Y. Sun, G. Lu, Q. Zhang, X. Chen and H. Zhang, Single-Layer MoS2 Phototransistors, *ACS Nano*, 2012, **6**, 74–80.

47 W. Choi, M. Y. Cho, A. Konar, J. H. Lee, G.-B. Cha, S. C. Hong, S. Kim, J. Kim, D. Jena, J. Joo and S. Kim, High-Detectivity Multilayer MoS2 Phototransistors with Spectral Response from Ultraviolet to Infrared, *Adv. Mater.*, 2012, **24**, 5832–5836.

48 O. Lopez-Sanchez, D. Lembke, M. Kayci, A. Radenovic and A. Kis, Ultrasensitive photodetectors based on monolayer MoS2, *Nat. Nanotechnol.*, 2013, **8**, 497.

49 D.-S. Tsai, K.-K. Liu, D.-H. Lien, M.-L. Tsai, C.-F. Kang, C.-A. Lin, L.-J. Li and J.-H. He, Few-Layer MoS2 with High Broadband Photogain and Fast Optical Switching for Use in Harsh Environments, *ACS Nano*, 2013, **7**, 3905–3911.

50 A. R. Klots, A. K. M. Newaz, B. Wang, D. Prasai, H. Krzyzanowska, J. Lin, D. Caudel, N. J. Ghimire, J. Yan, B. L. Ivanov, K. A. Velizhanin, A. Burger, D. G. Mandrus, N. H. Tolk, S. T. Pantelides and K. I. Bolotin, Probing excitonic states in suspended two-dimensional semiconductors by photocurrent spectroscopy, *Sci. Rep.*, 2014, **4**, 6608.

51 P.-L. Néstor, L. Zhong, R. P. Nihar, I.-R. Agustín, E. Ana Laura, M. Amber, L. Jun, M. A. Pulickel, T. Humberto, B. Luis and T. Mauricio, CVD-grown monolayered MoS 2 as an effective photosensor operating at low-voltage, *2D Mater.*, 2014, **1**, 011004.

52 M. Eginligil, B. Cao, Z. Wang, X. Shen, C. Cong, J. Shang, C. Soci and T. Yu, Dichroic spin–valley photocurrent in monolayer molybdenum disulphide, *Nat. Commun.*, 2015, **6**, 7636.

53 S. Ghosh, A. Winchester, B. Muchharla, M. Wasala, S. Feng, A. L. Elias, M. B. M. Krishna, T. Harada, C. Chin, K. Dani, S. Kar, M. Terrones, S. Talapatra and U. I. Photoresponse, Direct Evidence of Sub-gap States in Liquid Phase Exfoliated MoS2Thin Films, *Sci. Rep.*, 2015, **5**, 11272.

54 H. Wang, C. Zhang, W. Chan, S. Tiwari and F. Rana, Ultrafast response of monolayer molybdenum disulfide photodetectors, *Nat. Commun.*, 2015, **6**, 8831.

55 H. Yamaguchi, J.-C. Blancon, R. Kappera, S. Lei, S. Najmaei, B. D. Mangum, G. Gupta, P. M. Ajayan, J. Lou, M. Chhowalla, J. J. Crochet and A. D. Mohite, Spatially Resolved Photoexcited Charge-Carrier Dynamics in Phase-Engineered Monolayer MoS2, *ACS Nano*, 2015, **9**, 840–849.

56 J. Kwon, Y. K. Hong, G. Han, I. Omkaram, W. Choi, S. Kim and Y. Yoon, Giant Photoamplification in Indirect-Bandgap Multilayer MoS2 Phototransistors with Local Bottom-Gate Structures, *Adv. Mater.*, 2015, **27**, 2224–2230.

57 Z. Yang, R. Grassi, M. Freitag, Y.-H. Lee, T. Low and W. Zhu, Spatial/temporal photocurrent and electronic transport in monolayer molybdenum disulfide grown by chemical vapor deposition, *Appl. Phys. Lett.*, 2016, **108**, 083104.